The Journal of Experimental Biology 201, 91–102 (1998)
Printed in Great Britain © The Company of Biologists Limited 1998
JEB1163

PERIPHERAL ENCODING OF MOVING SOURCES BY THE LATERAL LINE SYSTEM OF A SIT-AND-WAIT PREDATOR

J. C. MONTGOMERY[1] AND S. COOMBS[2,*]

[1]*Experimental Biology Research Group, School of Biological Sciences, University of Auckland, Private Bag 92019, Auckland, New Zealand* and [2]*Parmly Hearing Institute, Loyola University of Chicago, 6525 North Sheridan Road, Chicago, IL 60626, USA*

*Author for correspondence (e-mail: scoombs@luc.edu)

Accepted 14 October 1997; published on WWW 9 December 1997

Summary

Video-tape recordings of prey-capture behaviour were made to demonstrate that stargazers can detect and capture prey in the dark and to determine the range of prey movement velocities that resulted in prey capture. Electrophysiological recording techniques were then used to determine how an artificial source (a sphere), moving at speeds within the range of recorded prey movement velocities, was encoded by anterior lateral line nerve fibres innervating the preopercular-mandibular canals on the head. A vibrating sphere was also used to measure frequency–response characteristics to determine the bandwidth of response and fibre origin (type of neuromast and location). In order to measure the relevant stimulus parameters likely to govern neural responses, the pressure-gradient pattern produced by the moving sphere was characterised with a pair of miniature hydrophones separated by approximately the same distance as head lateral line canal pores on stargazers. At least four different features of neural response patterns, including direction-dependent changes in the overall envelope of the firing rate pattern, could be predicted on the basis of measured pressure-gradient patterns. The dominant features of both the pressure-gradient and neural response patterns were produced by the wake behind the moving sphere, but behavioural observations indicated that stargazers were responding to the bow of an approaching prey, rather than its wake. Although the form of the wake behind the moving sphere is unlikely to be a good match for the stimulus mediating prey detection, these results clearly establish that pressure-gradient patterns are good predictors of neural response patterns. Thus, similar measurements of pressure-gradient patterns produced by more biologically relevant sources can be used to predict peripheral lateral line responses and stimulus features likely to be of key importance.

Key words: teleost, lateral line, peripheral encoding, stargazer, *Leptoscopus macropygus*, *Genyagnus monopterygius*.

Introduction

Fish have a mechanosensory lateral line which they use to monitor their hydrodynamic environment. One of the main functions of the lateral line is to detect the weak flow fields produced by the movements of other animals (Montgomery *et al.* 1995), including conspecifics (Partridge and Pitcher, 1980; Satou *et al.* 1987, 1994*a*,*b*) and prey (Enger *et al.* 1989; Hoekstra and Janssen, 1985; Montgomery, 1989; Montgomery and Milton, 1993).

Much of our understanding of how the lateral line system encodes subsurface flow fields comes from studies in which sinusoidally vibrating spheres (dipole sources) were used to characterise the response properties of peripheral lateral line nerve fibres (e.g. Montgomery, 1989; Coombs and Janssen, 1990). Since spheres can be vibrated sinuosoidally at different frequencies and since their flow fields can be easily measured and mathematically modelled, these dipole sources are particularly useful for a systems analysis of peripheral mechanics, for determining the frequency–response characteristics of the system, to distinguish between superficial and canal neuromast inputs, and for gaining a general understanding of peripheral physiology (e.g. Kroese and Schellart; 1992; Montgomery and Coombs, 1992; Coombs *et al.* 1996).

Although simple dipole sources can elicit naturally occurring feeding and orienting behaviours in some fish (Hoekstra and Janssen, 1985; Coombs and Janssen, 1990), this artificial stimulus by no means represents the full range of water motions likely to be biologically relevant to other, or even most, fish. As Bleckmann *et al.* (1995) point out, moving prey cause more complex hydrodynamic stimuli than do stationary vibrating spheres and, thus, other more quasi-natural stimuli, such as moving objects that can be manipulated and controlled in the laboratory, may provide new and important insights into how biologically relevant information is encoded

by the lateral line system. In the present study, we use both a standard dipole source and a sphere moving at constant velocity to investigate how the lateral line system of stargazers might encode moving sources, such as prey. In order to document the detection of moving prey by stargazers and to estimate some of the key features of prey movement that initiate successful feeding behaviour, we first made some preliminary observations of the feeding behaviour of stargazers under infrared light. We then recorded the response of anterior lateral line nerve fibres innervating the head lateral line system to a moving sphere that approximated the size and range of prey movement velocities observed during feeding behaviour.

Although peripheral and central lateral line responses to moving objects have been recorded in a number of different fish (the weakly electric fish *Eigenmannia* sp. Bleckmann and Zelick, 1993; catfish *Ancistrus* sp. and goldfish *Carassius auratus* Bleckmann *et al.* 1995; Müller *et al.* 1996; Mogdans *et al.* 1997), the present study differs from those in several respects. First, we have documented a biologically relevant context for the moving source in prey detection by stargazers and have confined our measurements to the range of source velocities likely to elicit feeding behaviour and to the part of the lateral line system (head canal system) likely to be involved in the behaviour. Second, we chose a sphere for our moving source, rather than the rectangular-shaped objects used in previous studies, since the flow patterns around this symmetrical source are relatively well known and, thus, more easily characterised and because spheres have also been used previously as vibrating sources to measure frequency–response characteristics. Third, we used a pair of miniature hydrophones, separated by approximately the same distance as the head lateral line canal pores on stargazers, to measure the pressure gradient pattern produced by the moving sphere. This approach has been used successfully in the past as a way of measuring the relevant stimulus parameters for a dipole source (Coombs *et al.* 1996), and we use it here to determine whether the same simulus parameters are relevant for moving sources.

In general, there will be a trade-off between choosing a stimulus that is complex but biologically relevant and one that is simple enough to characterise adequately. Our choice of animal, stimulus and measurement approach provides a quasi-natural context within which a well-characterised, but somewhat artificial, stimulus can be used to examine peripheral encoding in the lateral line system.

Materials and methods

Experimental animals

Animals were collected from the Whangateau estuary near the Leigh Marine Laboratory, University of New Zealand, using SCUBA. Owing to limitations in animal supply, behavioural observations were made on the estuarine stargazer (*Leptoscopus macropygus* Richardson), whereas physiological studies were conducted on the spotted stargazer (*Genyagnus monopterygius* Bloch and Schneider).

Behavioural methods

Estuarine stargazers were housed individually in indoor circular (1 m radius) tanks filled with sea water. The bottom of each tank was covered with a 10 cm layer of sand to allow the fish to bury themselves so that only their dorsal surface was evident. Water depth was approximately 20 cm. Observations of feeding behaviour were made at night under infrared illumination with an infrared-sensitive video camera positioned above the fish. Several yellow-eye mullet (*Aldrichetta forsteri* 80–120 mm standard length, SL, 15–20 mm maximum head width) were introduced into the tanks as prey fish at random locations. The approach tracks and velocities of the prey and the position of the prey at the time of strike were determined from the video record. Prey position and orientation were first taken at the time of the strike, and the video record was then reversed 10 frames at a time (=400 ms) to obtain the approach track of the prey. Approach velocities were determined from the distance travelled in this 400 ms period. The relatively shallow water depth, vertical camera position and limited field of view meant that swimming motions were essentially confined to and measured in the horizontal plane.

Stimulus generation and measurement

For the moving source used in physiological studies, a plastic sphere (7.5 mm radius) was mounted on the end of a rigid shaft, 10 cm long and 3 mm in diameter. The shaft was attached to the arm of an *x–y* plotter which moved the sphere in a linear motion parallel to and along the length of the fish. A voltage ramp to the plotter drove the sphere over a total range of 100–130 mm at a preselected speed.

The sound pressure associated with the moving source was measured with a pair of miniature hydrophones (B&K 8103) mounted together and centred on the range of movement. These hydrophones had a flat frequency response from 2 to 5000 Hz. The acoustic centres of the hydrophones (1 cm in diameter each) were separated by 11 mm, within the range of measured interpore distances on the preopercular-mandibular canals of the stargazers used in physiological experiments. This separation distance was used so that we could measure the pressure differences expected across pore pairs on the preopercular-mandibular canal of the stargazer. Pressure gradient measurements are predicated on the assumptions that (1) there is a single neuromast between every two pores on the canal and (2) the response of each neuromast (and afferent fibre) to fluid motions inside the canal is proportional to the outside pressure gradient across the two pores. Measurements were made with three different orientations of the hydrophone pair: parallel, orthogonal and 45 ° relative to the axis of source motion. Measurements were made in the physiological test tank at the same location as the fish, but in the absence of the fish. All other stimulus conditions were maintained identical to those used in physiological experiments. The time waveforms of the hydrophone outputs were averaged across eight stimulus cycles (fore and aft movement of the sphere), digitised

(1000 Hz sampling rate) and used to compute the final, averaged time waveform of the pressure differences between hydrophones.

For frequency–response analyses, a 4 mm radius bead was attached to a minishaker (Ling Dynamic Systems, model 200) driven by a power amplifier with input connections from the D/A output of a Labmaster interface card in a PC computer. The bead was vibrated sinusoidally at different frequencies with the edge of the bead approximately 4–6 mm from the skin surface. The axis of vibration was in a dorso-ventral direction, but parallel to the surface of the fish. The stimulus sequence was computer-generated to maintain a constant maximal acceleration over a range of frequencies between 7.4 and 208 Hz. The order of stimulus presentation was from high frequencies to low frequencies in three series (208–13 Hz, 167–10.4 Hz, 119–7.4 Hz). In each stimulus series, the duration of the stimulus was held constant such that the number of stimulus cycles ranged from 400 at the higher frequencies to 25 at the lower frequencies. The computer-generated waveform took the response dynamics of the minishaker into account. Correct calibration of the system was confirmed by recording the motion of the bead with an optoelectronic movement detector (PIN-Sc/10D photodetector, United Detector Technology).

Physiological methods

Before and during surgery, individual spotted stargazers were anaesthetised in 0.001 % MS-222 dissolved in sea water. To immobilise fish, a hole was drilled into the upper spinal cord canal and the cord was pithed with a flexible plastic rod. The drill was also used to open the dorsal cranium to expose the brain. For ethical reasons, the fish was then decerebrated by transection of the forebrain between the diencephalon and the telencephalon. The head was held firmly in a holder, and the fish was placed in an aquarium with the water level adjusted to just below the cranial opening. Fresh sea water in the aquarium was filtered and circulated through a cooler, which maintained the water temperature at 18–19 °C. Afferent unit activity was recorded at least 1 h after the transient use of MS-222. Evoked responses were recorded with sharp (approximately 20 MΩ) glass electrodes filled with 4 mol l^{-1} NaCl placed in the intracranial portion of the ventral branch of the anterior lateral line nerve. Experiments were performed under the authority of the Animal Ethical Committee at the University of Auckland.

Evoked responses were analyzed in the following way. Spike activity triggered standard 2 ms pulses from a window discriminator. The output of the window discriminator was then fed to the D/A input of the computer and used to generate a distribution of spike counts according to the time of occurrence during the entire period of stimulus presentation. Evoked responses to the moving sphere were based on peristimulus-time histograms (2 ms binwidth) for each movement direction, averaged over 20 repetitions of movement in each direction. Frequency responses to the vibrating sphere were based on period histograms (2 ms binwidth) for each cycle of vibration, averaged over a minimum of 25 cycles. Responsiveness to a given frequency was described in terms of the probability of a spike occurring at the same time (within a 2 ms bin) during the sinusoidal stimulus cycle. A perfectly phase-locked response, firing one spike per cycle at the same time during the cycle generates a probability of 1. No response generates a probability that is typically less than 0.1, depending on spontaneous activity. Response probability at each stimulus frequency (presented at 10–15 dB above threshold) was plotted as a function of frequency to generate a frequency–response curve for each fibre.

Results

Behaviour

Laboratory observations of estuarine stargazers under infrared light revealed that these fish bury themselves in the sand with only the anterior dorsal part of the body exposed. Prey movements over, or near, the head initiate a rapid strike at the prey. These observations in combination with field observations of both estuarine and spotted stargazers indicate that both stargazer species are lie-in-wait predators with similar prey-catching behaviour.

Eight successful strikes by two estuarine stargazers (SL=345 and 360 mm) were analysed from video records, four of which are presented in Fig. 1. All successful strikes occurred when the prey approached from the front of the predator and after the prey's head had passed over the exposed

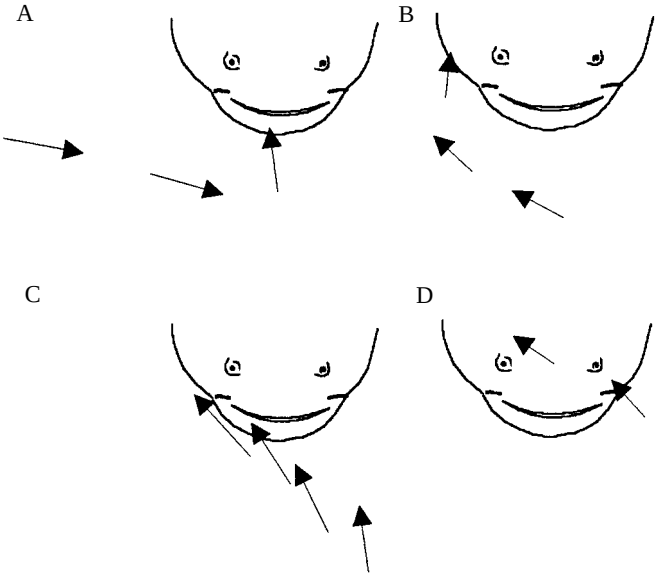

Fig. 1. Approach trajectory of prey during successful strikes by estuarine stargazers. The predator is buried in the sand with only the anterior dorsal part of the body exposed (head only shown). The arrows represent the position and the orientation of the prey. The tip of the arrow is at the snout of the prey and the base of the arrow is at the back of the prey's head (mid-dorsal line above the operculum). Arrows are shown at 400 ms intervals. The strike occurred when the prey was located at the position of the last arrow.

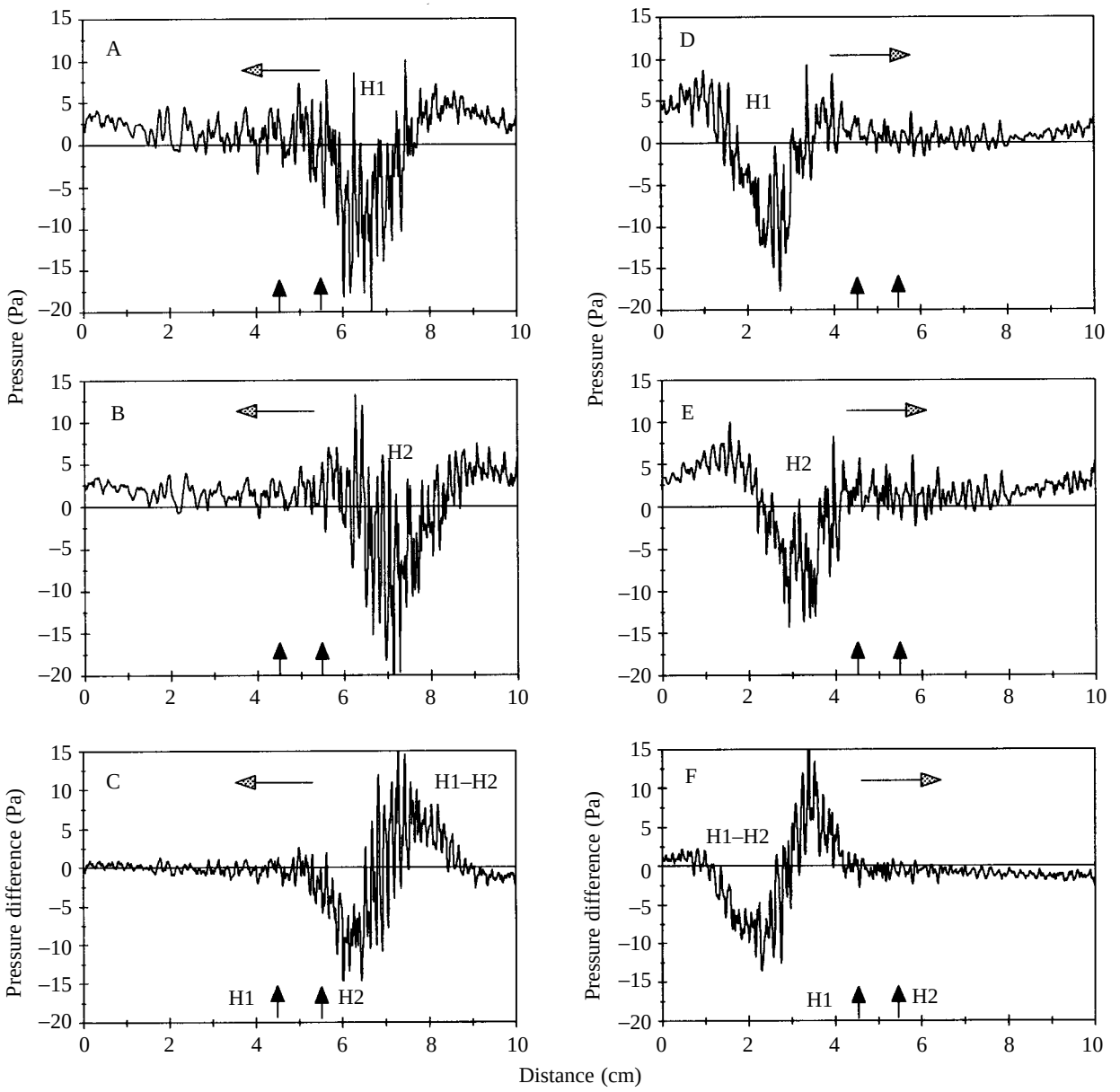

Fig. 2. Response waveform to the moving sphere from hydrophones 1 (H1) (A,D) and 2 (H2) (B,E) and the computed pressure difference (H1–H2) (C,F) to the moving sphere. All three waveforms are plotted as a function of source position (distance from the starting point, 0 cm) during the movement for forward (A–C) and backward (D–F) directions of motion. Elapsed time increases with distance along the *x*-axis of A–C, but decreases with distance along the *x*-axis of D–F. Arrows along the *x*-axis indicate the positions of the hydrophones. Source velocity 12 cm s^{-1}. Lateral distance of source from hydrophone pair 6 mm.

anterior edge of the stargazer as seen from above. The pathlength covered by the prey over the top of the stargazer (measured between the point at which the prey first intersects the anterior edge of the stargazer and the position of the prey snout at the time of strike initiation) was between 6 and 40 mm with a mean of 15 mm. Therefore, less than 40 % of the fish's total body length had passed over the stargazer's head at the time of strike initiation. Approach velocities ranged from 7 to 32.5 cm s^{-1} with a mean of 12.3±11.4 cm s^{-1} (mean ± S.E.M., N=7). Lack of resolution due to the dim infrared illumination precluded more detailed analysis of the approach trajectory.

Stimulus measurement

Fig. 2 shows the response waveforms of the simultaneously measured outputs from hydrophones 1 (H1) (Fig. 2A,D) and 2 (H2) (Fig. 2B,E) and the computed pressure difference (H1–H2) (Fig. 2C,F) as a function of source position (distance away from the starting position of 0 cm) for forward (Fig. 2A–C) and backward (Fig. 2D–F) directions of motion. In this example, the source was moving parallel to the hydrophone pair at a distance of 6 mm and at a velocity of 12 cm s^{-1}. In Fig. 3, the amplitude spectra for the pressure-difference records (H1–H2) are shown for the case in which

there was no source movement (Fig. 3A) and for source velocities of 6 cm s^{-1} (Fig. 3B), 12 cm s^{-1} (Fig. 3C) and 24 cm s^{-1} (Fig. 3D). Each spectrum was based on a waveform averaged over eight cycles (fore plus aft) of source movement.

These figures illustrate several key features of the source movement. One is that the resulting water motion is not smooth. The waveform fine structures (Fig. 2) all show a noise-like, alternating motion, which results in an increase in energy above ambient in spectral regions below approximately 100 Hz (Fig. 3C). A slight, but relatively broad, peak of energy near 80 Hz, most notable for source velocities of 12 and 24 cm s^{-1}, corresponds to the average periodicity of oscillations in the waveform fine structure after the source has passed the hydrophone pair (Fig. 2). These probably represent turbulence in the wake of the moving sphere, since they do not occur when the advancing source is in front of the hydrophone.

Noise levels are greatest below 40 Hz, and at least some of this noise is due to substratum-borne vibrations rather than the moving source, as shown by the amplitude spectrum in the absence of source movement (Fig. 3A) and as demonstrated in previous studies (e.g. Coombs *et al*. 1989). As source velocity increases from 6 to 24 cm s^{-1}, however, there is a predominant 20 dB increase in peak energy below 40 Hz and an upward spectral shift in its location from 1.5 to 6 Hz (Fig. 3B–D). This low-frequency shift corresponds to the low-frequency changes in the waveform envelope, which become higher in frequency (faster) as source velocity increases.

If we focus on the overall waveform envelope, rather than its fine structure, a second feature of the moving source is that there is a significant reduction in pressure after the source has passed each hydrophone. In the pressure-difference trace (H1–H2), this translates into a negative change in the pressure gradient followed by a positive change in the pressure gradient when the source moves in one direction and a positive change followed by a negative change when the source moves in the opposite direction (Figs 2, 4–6). Essentially, this means that the direction of the pressure gradient and thus the flow of water between the two hydrophones changes once each time the source moves past the pressure-gradient detector and that the direction of the change (positive-to-negative or negative-to-positive) depends on the direction of source movement.

Fig. 4A–C shows the effects of source velocity on the

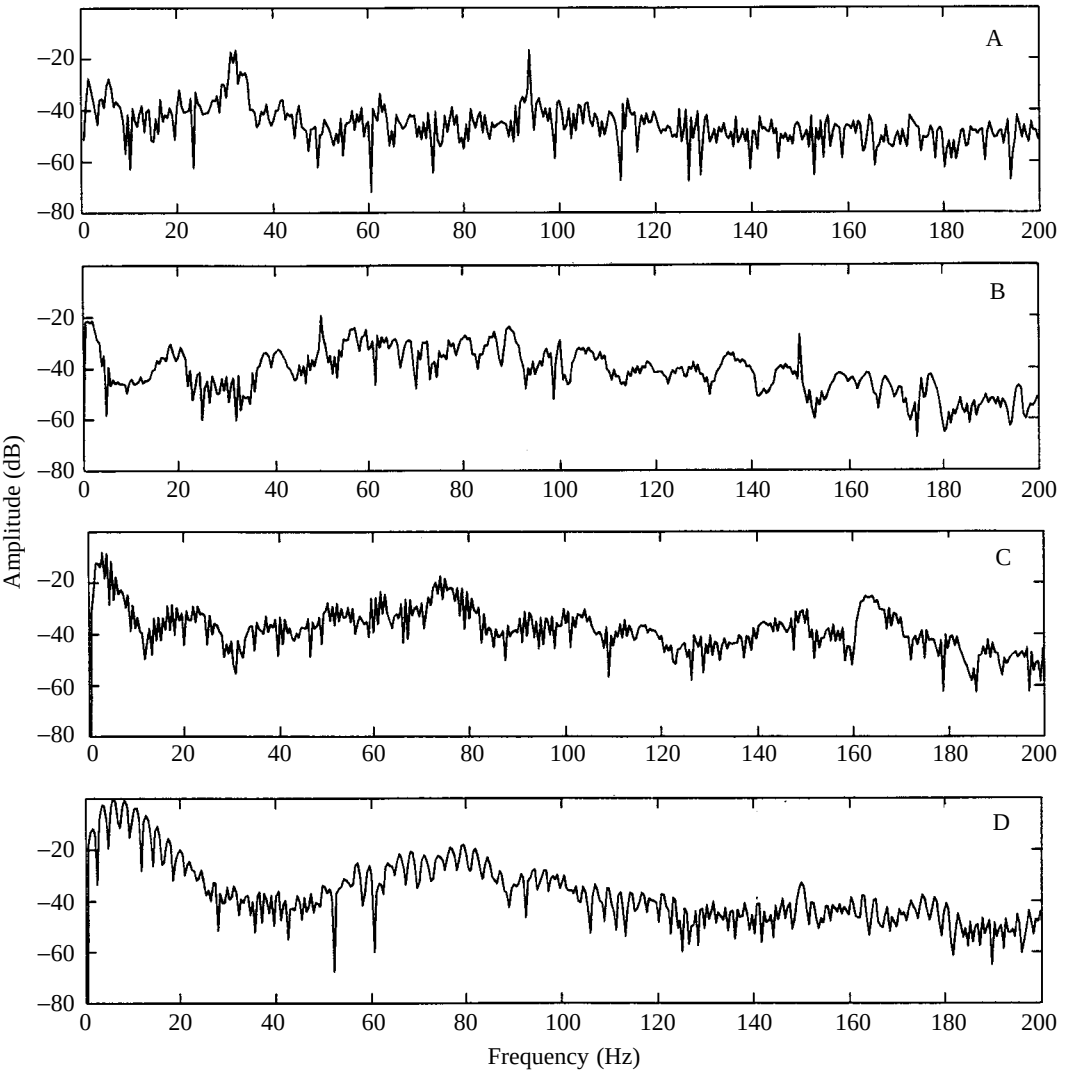

Fig. 3. Amplitude spectra of computed pressure difference for source velocities of 0 cm s^{-1} (A), 6 cm s^{-1} (B), 12 cm s^{-1} (C) and 24 cm s^{-1} (D). Amplitudes are normalized to 0 dB, which in this case is the peak amplitude in D for 24 cm s^{-1}.

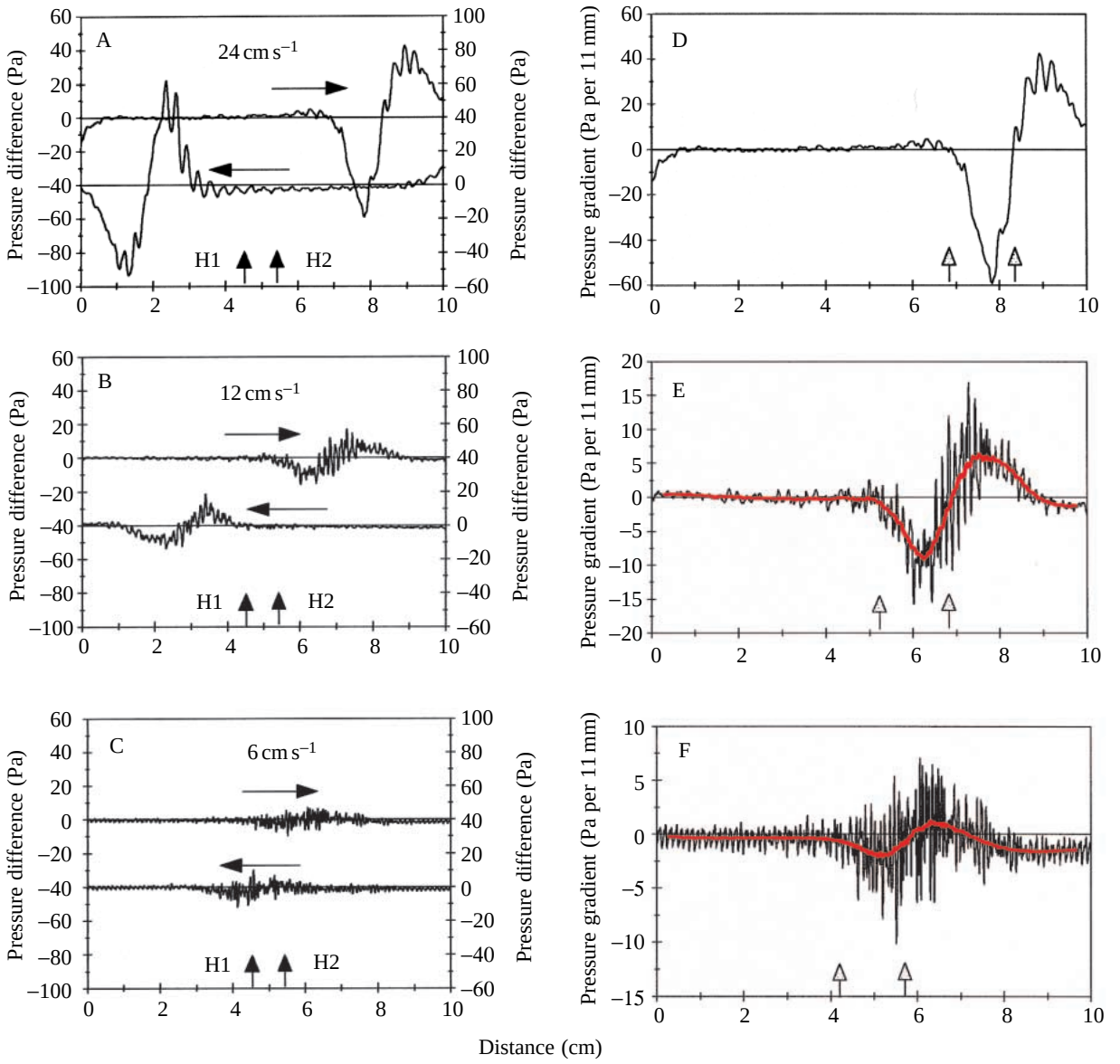

Fig. 4. (A–C) Pressure-difference waveforms produced by opposite directions of motion (see arrows above each waveform) for a source distance of 6 mm and source velocities of 24 cm s^{-1} (A), 12 cm s^{-1} (B) and 6 cm s^{-1} (C). Vertical arrows along the *x*-axis represent the positions of hydrophones 1 and 2, as in Fig. 2. Waveforms representing directions of motion towards increasing distances on the *x*-axis (top waveform) are plotted against the left-hand *y*-axis, whereas waveforms representing opposite directions (bottom waveform) are plotted against the right-hand *y*-axis. (D–F) Top waveforms in A, B and C replotted with vertical arrows along the *x*-axis indicating the spatial extent of the negative response peak in each case. Running averages of each waveform are plotted as thick red lines in E (averaging binwidth 50 ms per 0.5 cm) and F (100 ms per 0.5 cm binwidth) to emphasize low-frequency changes in the waveform envelope.

pressure-gradient waveform for each direction of motion. As velocity increases, pressure-gradient amplitudes increase. The distance lag of the peak pressure difference with respect to the hydrophone pair also increases. This can be seen most easily by observing the increasing spatial separation between the response peaks due to opposite directions of motion. Fig. 4D–F shows the spatial extent of the response, as measured from the beginning of the first negative-going peak to the beginning of the first positive-going peak (indicated by arrows along the *x*-axis for one direction only). To investigate the spatial extent of the waveform envelope, we plotted a running average (red thick line) of the response waveform (thin black line) to filter out the high-frequency oscillations. As Fig. 4D–F shows, the spatial extent of the response does not change with source velocity. These results are in direct contrast to those showing the effects of source distance on the pressure-gradient waveform (Fig. 5). In this case, as source distance decreases, the pressure difference amplitude increases (Fig. 5A–C) while the spatial extent of the response (Fig. 5D–F) decreases. Finally, Fig. 6 shows how various orientations of the

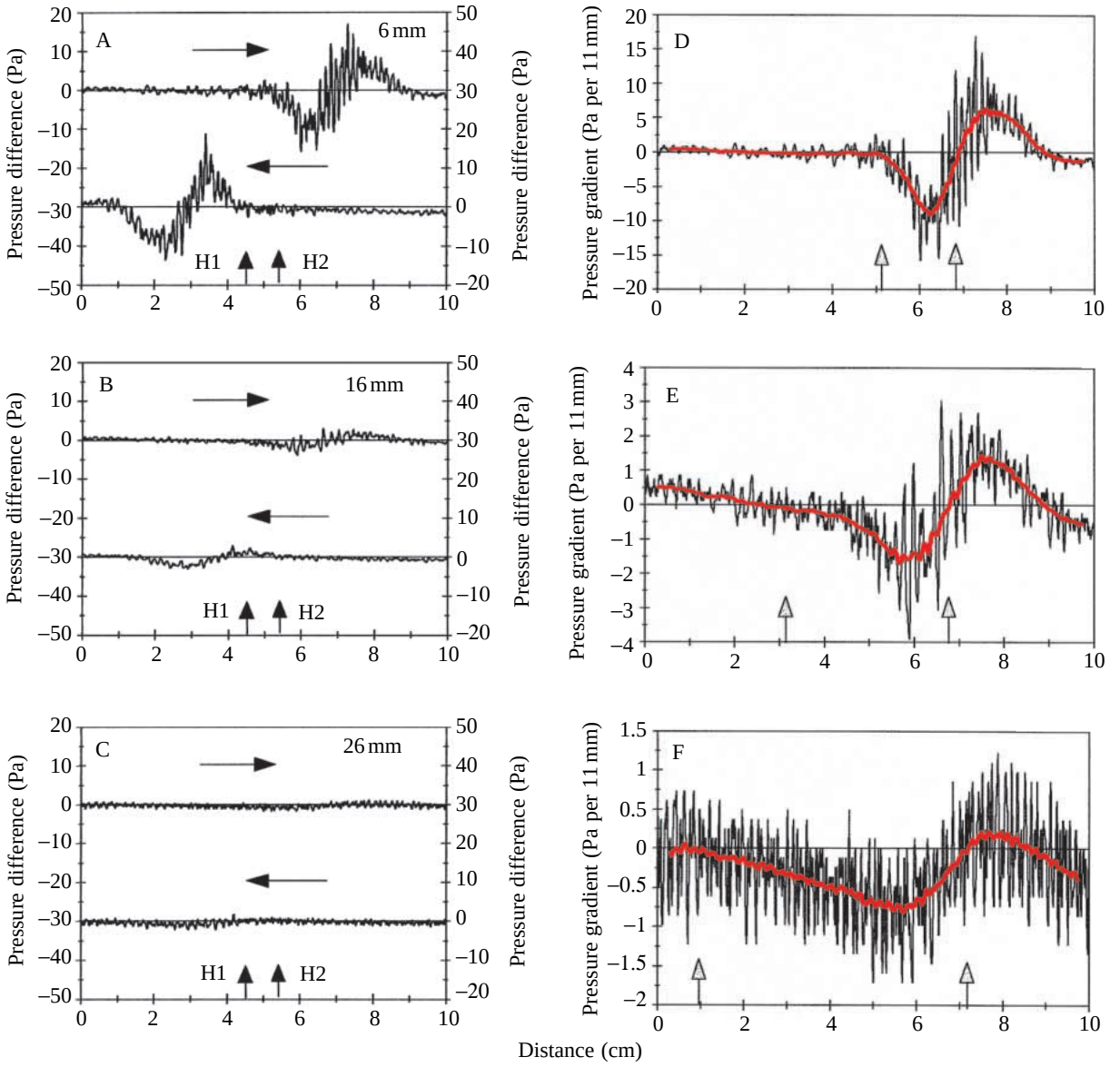

Fig. 5. Pressure-difference waveforms (A–C) corresponding to different source distances (source velocity constant at 12 cm s^{-1}) with the upper waveform replotted in each case on an expanded *y*-axis (D–F) as in Fig. 4.

hydrophone pair introduce asymmetrical changes in the overall waveform envelope for a source velocity of 12 cm s^{-1}.

Physiology

Data were obtained from 26 primary afferent fibres in the anterior lateral line nerve of two spotted stargazers (350 and 360 mm in SL). Responses from all of these fibres were localized to the region of the preopercular mandibular canal line by noting the source locations that created a 180 ° phase shift in the period histogram response to the vibrating sphere (Montgomery and Coombs, 1992). All were spontaneously active with a mean spontaneous rate of 35±6.1 impulses s^{-1} (mean ± S.E.M.).

Responses to the moving sphere in all fibres had several features in common that could be predicted from pressure-gradient measurements. One was the effect of motion direction on the overall pattern in the firing rate envelope. This effect was observed in all fibres, but is illustrated for two fibres responding to a range of source velocities at a fixed distance of 6 mm. For the fibre shown in Fig. 7B,C, posterior–anterior motion of the source with respect to the fish (as shown in Fig. 7A) caused an overall increase in the firing rate followed by an overall decrease in firing rate, whereas anterior–posterior movement had the reverse effect. The fibre shown in Fig. 8 had the same receptive field as the fibre illustrated in Fig. 7 (using the 180 ° phase shift criterion mentioned above), but a reversed polarity of response. Posterior–anterior movement caused a decrease followed by an increase in the overall firing rate.

A second feature that could be predicted in a general sense from pressure-gradient measurements is the fine structure of the firing rate response. Although we made no efforts to correlate the short-term firing rate fluctuations with the pressure-gradient fluctuations measured using the hydrophone pair, all fibres showed several cycles of firing rate increments and decrements embedded within the overall firing rate envelope that were consistent with the noise-like fluctuations in the fine structure of the pressure-gradient waveform (Figs 2, 4–6).

A third feature that could be predicted from pressure-gradient measurements was the effect of source velocity on the amplitude and location of excitatory response regions. The region of strongest response occurs after the source has passed the receptor (neuromast or hydrophone pair) location. Increasing the source velocity increases the peak firing rate and the distance lag between the source and the receptor at the time of the peak response. The latter can be most easily visualised and quantified by examining the spatial separation between excitatory response regions (i.e. overall increments in the firing rate) elicited by opposite directions of motion. For example, Figs 7B and 8B show that the peak-to-peak spatial separation between excitatory response regions elicited by anterior–posterior and posterior–anterior motion in these two fibres was approximately 3.5 cm for a 10.8 cm s^{-1} source velocity. In contrast, the spatial separation between excitatory response regions evoked by different directions of source

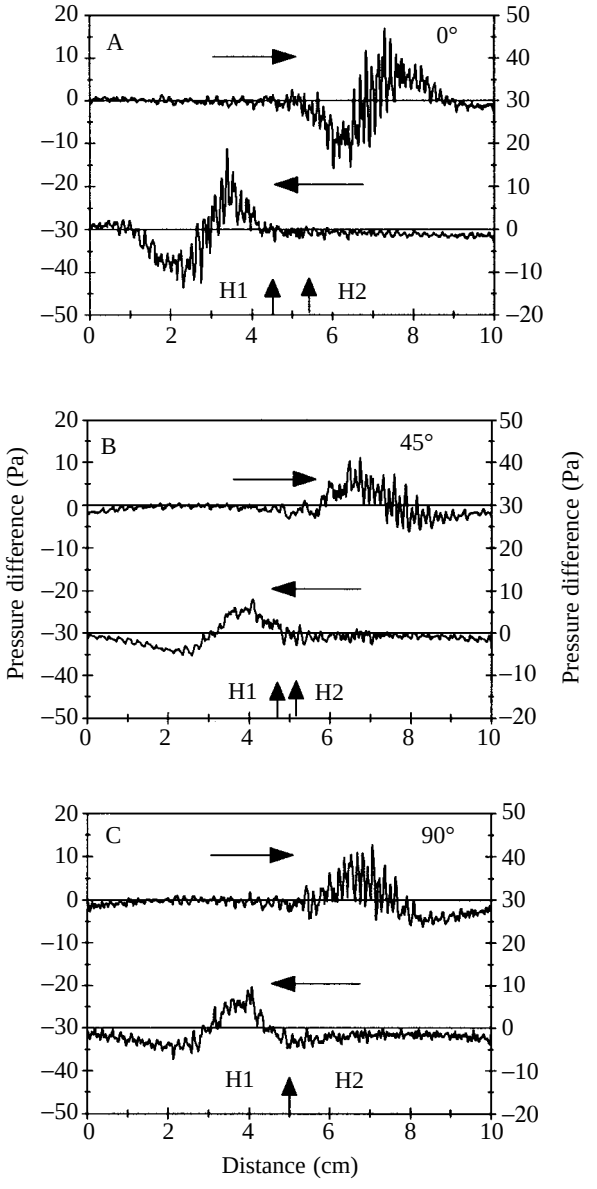

Fig. 6. Pressure difference waveforms as shown in Fig. 4B but for different orientations of the hydrophone pair (0 °, 45 ° or 90 °).

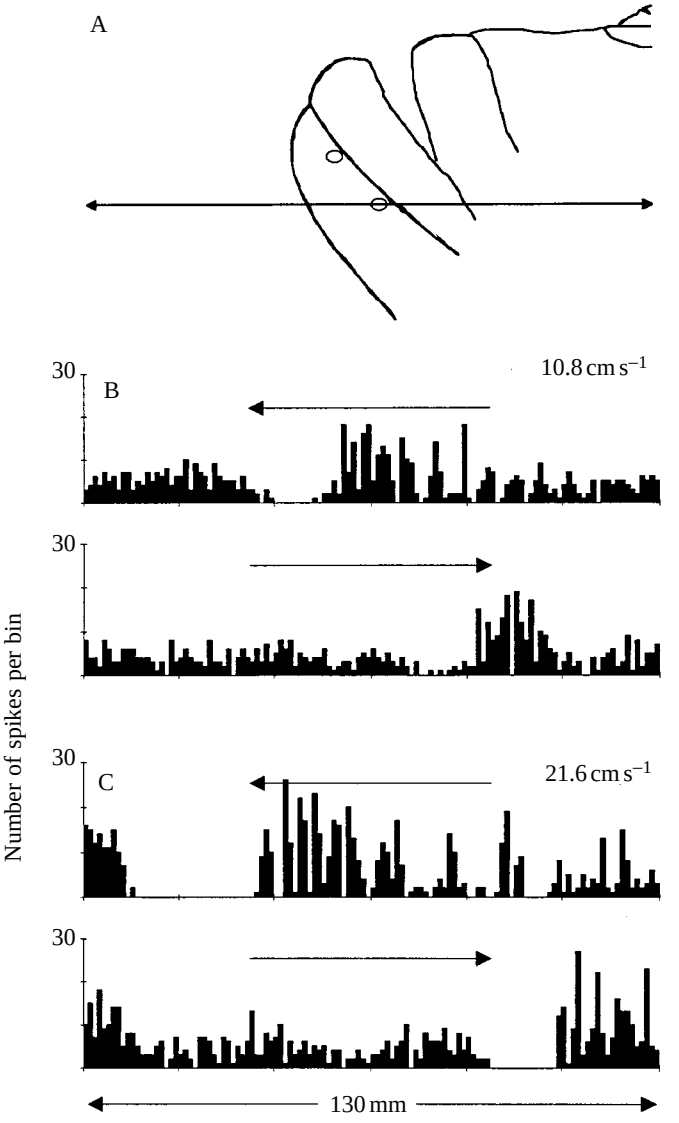

Fig. 7. Response of a mandibular lateral line nerve fibre to the moving stimulus. (A) Lateral view of the head of the stargazer showing the two pores between which a vibrating stimulus showed a 180 ° phase reversal. The position and extent of travel of the stimulus is shown by the arrow. (B) Stimulus histogram of the response of the fibre to the stimulus moving at 10.8 cm s^{-1} (2 ms bins, 20 repeat sweeps). (C) Stimulus histogram of the response of the fibre to the stimulus moving at 21.6 cm s^{-1} (2 ms bins, 20 repeat sweeps). The direction of movement of the stimulus is shown by the arrows.

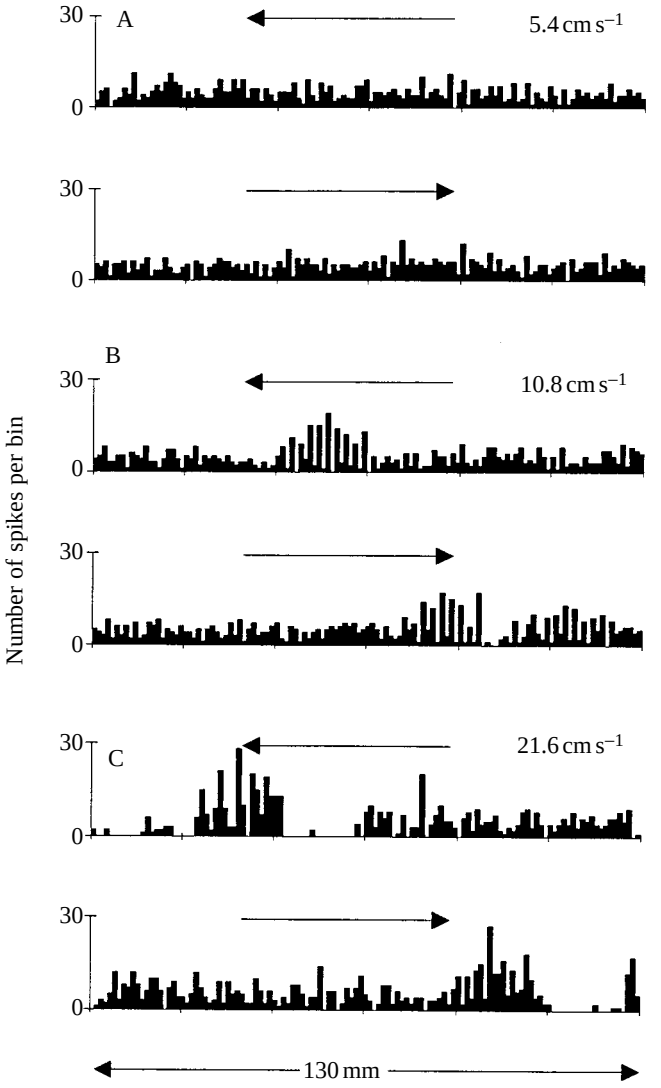

Fig. 8. Response of a fibre with a similar receptive field to that illustrated in Fig. 7. Details are as in Fig. 7. Note that this fibre has the opposite response polarity to that shown in Fig. 7.

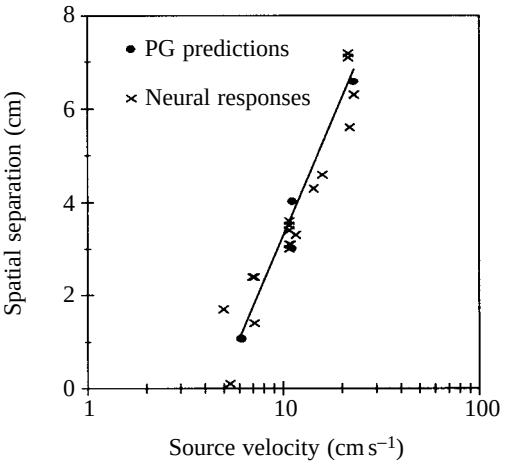

Fig. 9. Spatial separations between response peaks evoked by different directions of source motion for pressure-gradient (PG) predictions (filled circles) and neural responses (crosses) as a function of source velocity. Source distance was constant at 6 mm. The two PG predictions for a 12 cm s^{-1} source velocity indicate the range of separations to be expected between a 0 ° (upper circle) and 90 ° (lower circle) orientation of the hydrophone pair relative to the axis of source travel (see Fig. 6). The solid line describes a logarithmic function in which $SS=\log(V/4.9)\times10$, where SS is spatial separation (cm) and V is source velocity (cm s^{-1}). See text for further details.

movement at 21.6 cm s^{-1} was approximately 7.5 cm (Fig. 7C) and 6.4 cm (Fig. 8C) for these two fibres. These values correspond fairly well to spatial separations of measured pressure-gradient peaks of approximately 6.5 cm for a source velocity of 24 cm s^{-1} (Fig. 4A) and approximately 4 cm for a source velocity of 12 cm s^{-1} (Fig. 4B). Fig. 9 summarizes how spatial separation varies across fibres for different source velocities relative to our measured values for the hydrophone pair. As this figure shows, the spatial separation (distance lag between receptor and source) appears to be a logarithmic function of source velocity.

The fourth and final feature that could be predicted from pressure-gradient measurements is the general effect of source distance on the neural response. As Fig. 10 illustrates, increasing source distance results in a decrease in the amplitude of the neural response peak. Pressure-gradient patterns also predict that the spatial extent of the response will broaden with increasing source distance (Fig. 5D–F), but will not broaden as a function of source velocity (Fig. 4D–F). These effects are more difficult to quantify and compare at a population level without knowing the threshold of the fibre and where the stimulus level falls in the input/output function of the fibre. For example, a fibre that requires a pressure gradient of 10 Pa per 11 mm to reach threshold is likely to show a very narrow response peak to the 12 cm s^{-1} stimulus shown in Fig. 4E, but a much broader response peak to the 24 cm s^{-1} stimulus shown in Fig. 4D – the opposite of what might be predicted from the pressure-gradient measurements. Nevertheless, for the fibres illustrated in Figs 8 and 10, response peaks seem to cover a fairly constant spatial extent, of approximately 2.0 cm, for source velocities ranging from 10.8 to 21.6 cm s^{-1} (Fig. 8), whereas response peaks appear to broaden from approximately 2.6 cm to more than 4.0 cm for source distances ranging from 3 to 18 mm (Fig. 10).

In order to estimate the earliest possible neural response to sources moving at 10.8 cm s^{-1}, we measured the point at which the response rate exceeded the range of spontaneous rates in seven units. A response was detectable, on average, 66 ms before the stimulus passed over the response centre (i.e. the closest approach to the lateral line pore pair of interest), which at this speed represents a mean distance of 7.1±13.6 mm (N=7).

Finally, in order to confirm that fibres innervated canal neuromasts rather than superficial neuromasts, both of which are supplied by anterior lateral line nerve fibres, we also collected frequency–response data from eleven fibres, including those used to illustrate responses to moving sources (Figs 7, 8, 10). We used only data from canal neuromast fibres

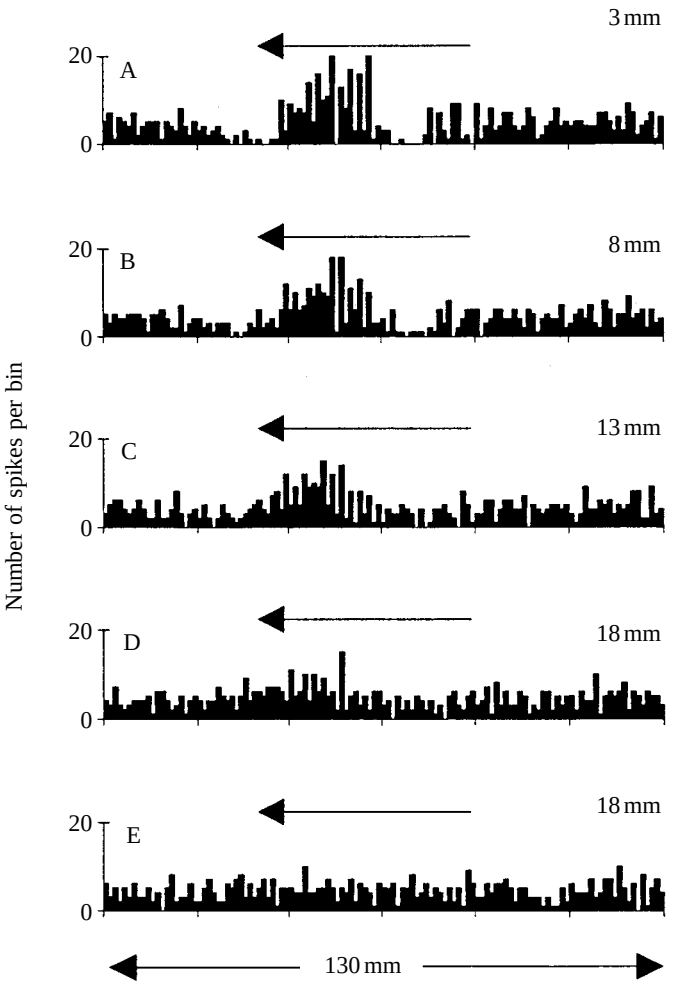

Fig. 10. Response of a fibre with its receptive field on the lower part of the mandible to a source movement of 10.8 cm s^{-1} with the moving stimulus situated at increasing distances from the surface of the fish. The arrows above the histograms indicate the direction of source movement.

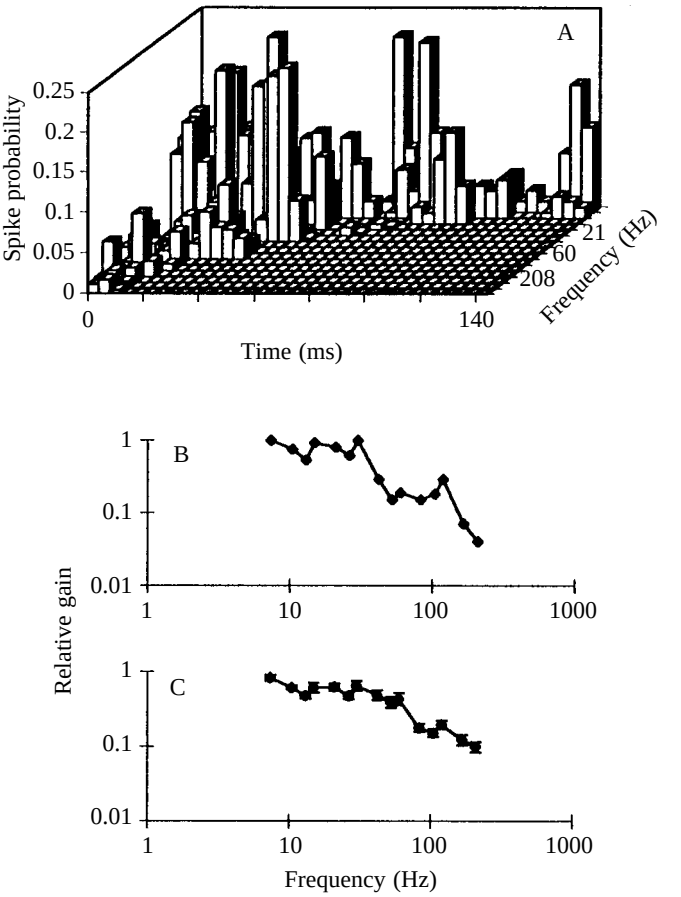

Fig. 11. Frequency–response analysis. (A) Three-dimensional histogram of the response of a single unit to 15 stimulus frequencies ranging from 7.4 to 208 Hz. Histogram height is the probability of a spike occurring in that particular time period. (B) Frequency–response characteristics of the same unit illustrated in A. Normalised peak spike-probability (relative gain) is plotted as a function of frequency. (C) Mean (± S.E.M.) frequency response of 11 lateral line units.

so that we could compare their responses with our pressure-gradient measures, using inter-hydrophone distances similar to interpore distances on the preopercular-mandibular canal of the stargazer (see Materials and methods).

Fig. 11A shows the responsiveness of a typical unit to sinusoidal vibrations of a sphere at different frequencies. Spike probability (*y*-axis) as a function of time during a single cycle of sinusoidal vibration (*x*-axis) is plotted as a function of frequency (*z*-axis). At low frequencies, the unit fired several spikes every stimulus cycle. The number of spikes per cycle declined until there were very few spikes at intermediate frequencies and 1 spike per cycle at the highest frequencies. The frequency response curve for this unit is shown in Fig. 11B. The response is consistent with the expected frequency response of a canal neuromast to fixed acceleration amplitudes, showing a relatively flat frequency response at low frequencies, which declines at frequencies higher than approximately 40–50 Hz. The frequency response characteristics of different units were relatively consistent, and the mean response (± S.E.M.) is shown in Fig. 11C, demonstrating that these fibres probably innervated canal rather than superficial neuromasts. The mean characteristic frequency (the frequency at which the response rate decreased to 71 % of maximum) of these units was 36±18.3 Hz.

Discussion

The responses of peripheral lateral line fibres in the stargazer to a moving object are very similar to those reported for peripheral fibres in *Eigenmannia* sp. (Bleckmann and Zelick, 1993). Similarities include (1) direction-dependent patterns in the overall envelope of the firing rate pattern such that source movement in one direction causes a general increase in the firing rate followed by a general decrease, whereas movement in the opposite direction causes an overall decrease followed by an overall increase, (2) fine-structure changes in the firing rate such that there are several cycles of firing rate increments

and decrements embedded within the overall envelope of the response pattern described above, and (3) peak firing rates that increase with increasing source velocity and decreasing source distance.

The use of a moving sphere and the more extensive stimulus characterisation undertaken in the present study clearly demonstrate three things. First, is that the pressure-gradient pattern is a very good predictor of peripheral lateral line nerve responses. Pressure-gradient changes measured for the moving source can predict several features of the neural response patterns, including (1) direction-dependent changes in the overall envelope of the firing rate pattern, (2) fine-structure fluctuations in the firing rate, (3) increasing distance lags between the source and the receptor at the time of the peak response as a function of increasing source velocity, and (4) neural response peaks that increase in their maximum firing rate as a function of increasing source velocity as well as decreasing source distance. These findings, in combination with findings from previous studies on the responses of peripheral lateral line fibres to sinusoidally vibrating spheres (Coombs *et al*. 1996; Coombs and Conley, 1997), indicate that pressure-gradient patterns are good predictors of neural responses under a variety of stimulus conditions.

A second major feature of these results is that the overall increase in energy above ambient noise levels and the upward shift of peak (low-frequency) energy that occurs when source velocity increases from 6 to 24 cm s^{-1} (Fig. 3) are well within the detection bandwidth of the lateral line system of the stargazer (Fig. 11B,C). It is most likely that energy peaks below 10 Hz are due to the large pressure-gradient changes in the overall waveform envelope, since the period associated with a single cycle of these large changes (Fig. 4D–F) predicts quite accurately the upward shift of peak energy observed in the amplitude spectra (Fig. 3B–D). By the same token, the average period associated with fluctuations in the fine structure of the waveform approximates the secondary energy peaks located between 40 and 100 Hz. To the extent that the amplitude spectrum of a moving sphere will reflect that of a moving prey, detection of waveform fine structure would almost certainly be mediated by canal, rather than superficial, neuromasts. This conclusion is based on the fact that canal neuromast fibres have been shown in the present study (Fig. 11B,C) and by others (e.g. Montgomery and Coombs, 1992) to respond equally well to constant-acceleration stimuli over a relatively wide range of frequencies from below 10 Hz to an upper cut-off frequency ranging from 30 to 100 Hz, depending on the species. In contrast, superficial neuromast fibres respond best to lower frequencies, with responsiveness declining in proportion to increasing frequency.

A final major feature of these results is that the primary stimulus generated by a sphere moving at constant velocity is the wake generated behind it. Thus, it is the wake that generates the large (envelope) changes in the pressure-gradient waveform and probably the turbulence in the wake that generates the more random, high-frequency oscillations in the waveform fine structure. At the Reynolds numbers operating in these experiments (Re=6×10^2 to 2.4×10^3), the wake behind a sphere will be generated as the flow collapses back into the space generated by the passage of the sphere. This occurs 2–3 diameters behind the sphere, which is where the major pressure gradient occurs (Figs 2, 4–6). To this extent, the lateral line responses observed to the passage of a moving sphere, a non-streamlined object, will not be representative of those generated by a passing fish. For example, the streamlined shapes of fish should result in dramatically reduced wake widths. In addition, fish that swim using subundulatory patterns have been shown to shed a chain of vortices behind the caudal edge of the tail fin with each tail flick (Blickhan *et al*. 1992). Nevertheless, measurements of water velocities produced in the wake of swimming fish indicate that even these biologically significant wakes can be broadband and contain energy in the same frequency range (up to 100 Hz) (Bleckmann *et al*. 1991) as the wake of our moving sphere.

Our behavioural observations, however, suggest that stargazers are capable of responding to the water motions created by an approaching fish and, thus, they do not necessarily rely on the wakes generated by fish that have already passed. Indeed, several fish species have been shown to have highly directed bites in response to artificial sources, such as water jets (Janssen *et al.* 1990; Janssen and Corcoran, 1993) and moving spheres (Janssen, 1996), both of which may approximate the bow pressure wave of an approaching fish. If, instead of concentrating on the dominant response to the sphere's wake, we focus attention on the earliest response detectable in the primary afferents, this would give an estimate of how far in advance of its approach the lateral line could detect the bow of the advancing sphere. The results show that, on average, a response to a 10.8 cm s^{-1} stimulus occurs by approximately 66 ms, or 7.1 mm in advance of the stimulus arriving at the receptor pore. Thus, the effective range of the lateral line for this type of stimulus is relatively short. Given that, in general, the prey has crossed the lateral edge of the stargazer by approximately 15 mm at the time of strike initiation, this gives a strike latency of only approximately 200 ms from the time of first prey detection. These are only rough estimates, but do indicate that a rapid decision/execution network must be in operation for lateral-line-mediated predation in the stargazer.

These estimates of distance ranges and strike latencies are based on the simplifying assumption that prey move at constant velocities. The distance range of detection or the strike latency could easily be altered by features of the prey movement that generate a stronger stimulus than that produced by a constant velocity of movement. It is perhaps significant that the two strikes occurring in relation to the shortest pathlengths (Fig. 1A,B) are those that are preceded by a rapid turn of the prey in the approach track. These rapid turns are undoubtedly associated with a significant acceleration component and, to the extent that this is important in prey detection, the constant-velocity source used in physiological experiments is dissimilar to more biologically relevant signals.

As the above considerations demonstrate, the choice of the stimulus for studying lateral line central-processing mechanisms is particularly important. It is likely that the functional attributes

of the central networks will only be revealed when they are operating at something close to their normal operating ranges. The wake produced behind a moving sphere appears to dominate the peripheral lateral line response, but it may not be particularly important for prey detection by the stargazer or for other lateral-line-mediated behaviours. By the same token, it will be difficult to determine how central networks enhance or transform information encoded at the periphery without a firm understanding of how the periphery transforms or encodes the hydrodynamic stimulus field. The latter is more difficult to achieve with biologically relevant signals, which are complex and difficult to control under experimental conditions. Thus, there will always be a trade-off between choosing a stimulus that is biologically relevant yet simple enough to control and characterise adequately. Although the moving sphere used in the present study does not accurately represent all features of the live prey detected and captured by the stargazer, it does provide a means by which we could demonstrate for the first time how the lateral line periphery transforms the hydrodynamic stimulus field of a moving source with turbulent wakes. As we continue to obtain evidence for the pressure-gradient model of peripheral transduction of hydrodynamic stimuli, predictions of how the lateral line system responds to more biologically relevant and complex stimuli will become easier since pressure-gradient patterns around live sources can be measured more easily than the neural responses evoked by them.

The study was supported by the Office of Naval Research and by the University of Auckland Research Committee. We would like to thank Dr Joachim Mogdans for his comments and suggestions on an earlier draft of this paper.

References

BLECKMANN, H., BREITHAUPT, T., BLICKHAN, R. AND TAUTZ, J. (1991). The time course and frequency content of hydrodynamic events caused by moving fish, frogs and crustaceans. *J. comp. Physiol.* A **168**, 749–757.

BLECKMANN, H., MOGDANS, J. AND FLECK, A. (1995). Integration of hydrodynamic information in the hindbrain of fishes. *Mar. fresh. Behav. Physiol*. **27**, 77–94.

BLECKMANN, H. AND ZELICK, R. (1993). The responses of peripheral and central mechanosensory lateral line units of weakly electric fish to moving objects. *J. comp. Physiol.* A **172**, 115–128.

BLICKHAN, R., KRICK, C., ZEHREN, D. AND NACHTIGALL, W. (1992). Generation of a vortex chain in the wake of a subundulatory swimmer. *Naturwissenschaften* **79**, 220–221.

COOMBS, S. AND CONLEY, R. A. (1997). Dipole source localization by the mottled sculpin. II. The role of lateral line excitation patterns. *J. comp. Physiol*. **180**, 401–415.

COOMBS, S., FAY, R. R. AND JANSSEN, J. (1989). Hot-film anemometry for measuring lateral line stimuli. *J. acoust. Soc. Am.* **85**, 2185–2193.

COOMBS, S., HASTINGS, M. AND FINNERAN, J. (1996). Modeling and measuring lateral line excitation patterns to changing dipole source locations. *J. comp. Physiol.* A **178**, 359–371.

COOMBS, S. AND JANSSEN, J. (1990). Behavioral and neurophysiological assessment of lateral line sensitivity in the mottled sculpin, *Cottus bairdi*. *J. comp. Physiol.* A **167**, 557–567.

ENGER, P. S., KALMIJN, A. J. AND SAND, O. (1989). Behavioral investigations of the functions of the lateral line and inner ear in predation. In *The Mechanosensory Lateral Line: Neurobiology and Evolution* (ed. S. Coombs, P. Gorner and H. Muntz), pp. 575–587. New York: Springer-Verlag.

HOEKSTRA, D. AND JANSSEN, J. (1985). Non visual feeding behavior of the mottled sculpin. *Env. Biol. Fish.* **12**, 111–117.

JANSSEN, J. (1996). Use of the lateral line and tactile senses in feeding in four antarctic nototheniid fishes. *Env. Biol. Fish*. **47**, 51–64.

JANSSEN, J., COOMBS, S. AND PRIDE, S. (1990). Feeding and orientation of mottled sculpin, *Cottus bairdi*, to water jets. *Env. Biol. Fish*. **29**, 43–50.

JANSSEN, J. AND CORCORAN, J. (1993). Lateral line stimuli can override vision to determine sunfish strike trajectory. *J. exp. Biol*. **176**, 299–305.

KROESE, A. B. A. AND SCHELLART, N. A. M. (1992). Velocity- and acceleration-sensitive units in the trunk lateral line of the trout. *J. Neurophyiol.* **68**, 2212–2221.

MOGDANS, J., BLECKMANN, H. AND MENGER, N. (1997). Sensitivity of central units in the goldfish, *Carassius auratus*, to transient hydrodynamic stimuli. *Brain Behav. Evol.* (in press).

MONTGOMERY, J. C. (1989). Lateral line detection of planktonic prey. In *The Mechanosensory Lateral Line: Neurobiology and Evolution* (ed. S. Coombs, P. Gorner and H. Muntz), pp. 561–574. New York: Springer-Verlag.

MONTGOMERY, J. C. AND COOMBS, S. (1992). Physiological characterization of lateral line function in the Antarctic fish, *Trematomus bernacchii*. *Brain Behav. Evol.* **40**, 209–216.

MONTGOMERY, J. C., COOMBS, S. AND HALSTEAD, M. B. D. (1995). Biology of the mechanosensory lateral line in fishes. *Rev. Fish Biol. Fish.* **5**, 399–416.

MONTGOMERY, J. C. AND MILTON, R. C. (1993). Use of the lateral line for feeding in the torrentfish (*Cheimarrichthys fosteri*). *N.Z. J. Zool*. **20**, 121–125.

MÜLLER, H. M., FLECK, A., AND BLECKMANN, H. (1996). The responses of central octavolateralis cells to moving sources. *J. comp. Physiol.* **179**, 455–473.

PARTRIDGE, B. L. AND PITCHER, T. J. (1980). The sensory basis of fish schools; relative roles of lateral line and vision. *J. comp. Physiol.* **135**, 315–325.

SATOU, M., TAKEUCHI, H. A., NISHII, J., TANABE, M., KITAMURA, S., OKUMOTO, N. AND IWATA, M. (1994*a*). Behavioral and electrophysiological evidence that the lateral line is involved in the inter-sexual vibrational communication of the hime salmon (landlocked red salmon, *Oncorhynchus nerka*). *J. comp. Physiol.* A **174**, 539–549.

SATOU, M., TAKEUCHI, H. A., TAKEI, K., HASEGAWA, T., MATSUSHIMA, T. AND OKUMOTO, N. (1994*b*). Characterization of vibrational and visual signals which elicit spawning behavior in the male hime salmon (landlocked red salmon, *Oncorhynchus nerka*). *J. comp. Physiol.* A **174**, 527–537.

SATOU, M., TAKEUCHI, H., TAKEI, K., HASEGAWA, T., OKUMOTO, N. AND UEDA, K. (1987). Involvement of vibrational and visual cues in eliciting spawning behaviour in male Hine salmon (landlocked red salmon, *Oncorhynchus nerka*). *Anim. Behav*. **35**, 1556–1584.